RSC Advances

PAPER

View Article Online
View Journal | View Issue

Cite this: *RSC Adv.*, 2023, **13**, 9195

Polydopamine-assisted tranilast immobilization on a PLA chamber to enhance fat flaps regeneration by reducing tissue fibrosis

Zhangsong Peng, †[a] Qiang Chang, †[a] Xilong Liu,†[b] Danni Chen,[a] Feng Lu*[a] and Xihang Chen*[a]

Tissue engineering chambers (TECs) have been shown to be useful in regenerating adipose tissue. However, tissue fibrosis caused by the chambers compromises the final volume of the newly formed adipose tissue. Surface modifications can compensate for the lack of biocompatibility of an implant. Tranilast (Tra) is an antifibrotic drug used to treat fibrotic pathologies, including keloids and scleroderma. In this study, a polydopamine-assisted tranilast coating (pDA + Tra) was prepared on a polylactic acid (PLA) chamber to minimize tissue fibrosis and achieve a large volume of fat flap regeneration. The *in vitro* results showed that, in contrast to a PLA chamber, roughness increased, and the fibroblast adhesion and smooth muscle antibody-positive immunoreactivity decreased in the PLA + pDA + Tra chamber. In addition, pedicled adipose tissue flaps were separated from the back of the rabbit and inserted into each chamber using the classic TEC procedure. After 16 weeks, the marked attenuation of fibrosis and promotion of fat regeneration was observed in the PLA + pDA + Tra chamber in contrast to the PLA chamber. Moreover, in contrast to the PLA chamber, Q-PCR results showed that fibrotic factor TGF-β was significantly reduced, associated with a remarkable increase in adipogenic differentiation transcription factors PPAR-γ and C/EBPα in the PLA + pDA + Tra chamber after 16 weeks ($p < 0.05$). Thus, PLA chambers loaded with pDA + Tra on the surface have good biocompatibility, and chemical anti-fibrosis reagents can synergistically reduce fibrosis formation while excellently promoting adipose tissue regeneration.

Received 21st August 2022
Accepted 22nd February 2023

DOI: 10.1039/d2ra05237g

rsc.li/rsc-advances

1. Introduction

Breast cancer ranks as the highest in morbidity among female tumors.[1] Conventional treatments include the transfer of autologous skin-fascia-muscle flaps,[2] implantation of breast prostheses,[3] or transplantation of autologous fat.[4] However, technical difficulties, secondary injuries, and mediocre appearance hinder the widespread reconstruction of these large defects.[5,6]

Tissue engineering chamber (TEC) technology offers a new paradigm for the reconstruction of large defects. When the original vascular ring or pedicled fat flap is transferred into a flexible silicone chamber with prescriptive three-dimensional space, mature adipose tissue can regenerate *de novo* in this bio-incubator in an adipogenesis environment.[7–10] However, there are still some obstacles to achieving the ideal outcome, such as fibrosis formation around and within the newly formed tissue.[10,11] Fibrosis is associated with poor expandability and impaired function of adipose tissue. Therefore, a new approach should be taken in the selection of materials, and reprocessing strategies should be developed to prevent fibrosis formation in the built-in chamber.

These chamber materials used in clinical applications should meet the following requirements: good biocompatibility, degradability along with non-toxic by-products, solid mechanical resistance to skin tension during the remodeling and regeneration process, and ready-to-use, or highly customizable.[12] In particular, polylactic acid (PLA) has been approved by the FDA and is widely used due to its good biocompatibility, biodegradability, and solid support. It is used in various medical products such as absorbable sutures, drug delivery carriers, bone implants, screws, and tissue engineering scaffolds.[13–15] Owing to its thermoplastic properties and fused deposition modeling, PLA filaments can be manufactured to the desired dimensions using a sophisticated 3D printing technique, allowing convenience, rapid prototyping, and personalization.

However, after implantation, degradable materials can also cause tissue fibrosis, similar to non-absorbable materials.[16]

[a]*Department of Plastic and Cosmetic Surgery, Nanfang Hospital, Southern Medical University, 1838 Guangzhou North Road, Guangzhou, Guangdong 510515, China. E-mail: XihangChen@hotmail.com; doctorlufeng@hotmail.com; Fax: +86 (020) 61641869; Tel: +86 (020) 61641869*

[b]*Department of Medical Imaging Center, Nanfang Hospital, Southern Medical University, Guangzhou, China*

† These authors contributed equally and considered as co-first authors.

Chamber-induced tissue fibrosis is strongly influenced by surface properties, such as roughness, texture, surface free energy, surface charge, and chemical composition.[17] In the process of tissue fibrosis formation, the most critical biological behavior is the recruitment of fibroblasts and their subsequent polarization into myofibroblasts.[18] Transforming growth factor-β (TGF-β) is a crucial soluble cytokine that mediates fibrotic cascades by inducing myofibroblast activation.[19] Activated myofibroblasts form a positive feedback loop by secreting TGF-β, which further exacerbates fibrosis.[20] Surface roughening treatment has been shown to reduce fibroblast activity, but this type of physical treatment appears to produce more remarkable results using other interventions.[21]

As a drug commonly used in clinical practice, tranilast has been shown to inhibit TGF-β-mediated fibrosis in various tissues and was approved in 1993 for the treatment of keloids and hypertrophic scars.[22,23] According to previous reports, a low dose of tranilast (30–300 μM) can suppress fibroblast proliferation, which mainly relies on the suppression of the TGF-β1 receptor to terminate the cascade signal.[24,25] Therefore, we propose to establish a physical roughening chamber with chemical tranilast coating. To increase the efficiency, polydopamine (pDA) was chosen to form a thin membrane on the chamber surface because it self-polymerizes in a slightly alkaline environment and can universally adhere to biomolecules. This combination is expected to further attenuate capsule formation and lead to large-scale adipose tissue regeneration.

In the present study, the PLA filament was first printed with a commercial 3D printer for chamber construction with the primary dimension, and the surface was roughened with a special sandpaper; then, the polydopamine layer was applied to the chamber surface and then bonded with tranilast. The principle of this design was to meet the requirements of space mechanics, further suppressing the behavior of cells along with TGF-β-mediated fibrosis, and create a preferential adipogenic environment to realize large-volume adipose tissue regeneration. Harvested neo-tissues were assessed by magnetic resonance imaging (MRI), histological examination, Q-PCR, and quantitative evaluation of collagen and α-smooth muscle actin (α-SMA).

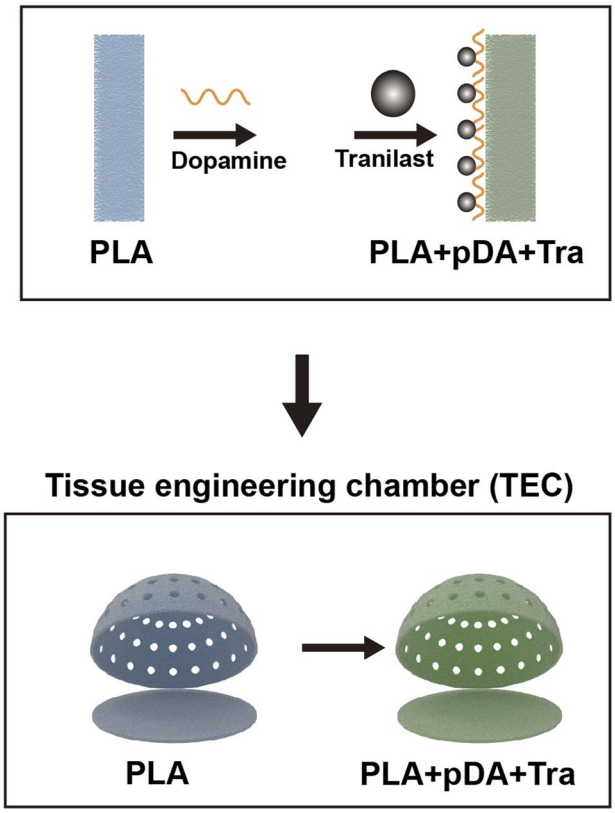

Fig. 1 Schematic of the fabrication process for the PLA + DA + Tra chamber.

2. Materials and methods

2.1 Construction and mechanical properties of the PLA chamber

The hollow hemispherical chamber with a radius of 15 mm and a whole volume of 6.75 ml was modeled using Solidworks. Circular windows were designed on the spherical surface to enhance nutrient transport between the inner and outer sides of the chamber (Fig. 1). The 3D printer was purchased from Creality Corp. (Ender V2, Shenzhen, CN) with the corresponding PLA filament (diameter of 1.75 mm), and the extruder and platform temperatures were set to 205 and 60 °C, respectively, to ensure fluent squeezing and stable adhesion. Then, the surface of the PLA chambers was roughened with 320-grit sandpaper. The PLA chamber roughened with sandpaper was used as a control group.

A bending test was performed on the samples using a universal testing machine (CTS-E100, Zwick, GER) with a support plate of 100 mm and a speed of 2 mm min^{-1}; the test was terminated when the displacement reached 5 mm. The load–displacement curve was recorded, and the maximum load and stiffness of each sample were calculated. Five samples were tested for each group.

2.2 Polydopamine (pDA) coating and tranilast (Tra) adhesion on the chamber surface

The pDA coating procedure was performed according to a previous report.[26] The PLA chambers were soaked in dopamine solution (2 mg ml^{-1} in 10 mM Tris-HCl, pH 8.5) and shaken gently on an oscillator for 2 h at 37 °C. To remove free dopamine, the pDA-coated rough PLA chambers were washed five times with deionized water. Tranilast (0.5 w/v in DMSO) was then added to the PLA + pDA chambers and incubated for an additional 12 h. The substrates were washed three times with deionized water to remove free tranilast. PLA without pDA coating was also used to adsorb tranilast.

2.3 Fourier transform infrared spectroscopy (FTIR)

Samples of PLA, PLA + pDA, PLA + Tra, and PLA + pDA + Tra were recorded using an FTIR spectrometer (Vertex 70; Bruker, Billerica, MA, USA) using the KBr method to investigate the presence of pDA or tranilast after coating. For this assay,

dopamine and tranilast were milled with potassium bromide (KBr) to produce a fine powder, which was then compressed into thin slices for analyses. At least three samples were analyzed for each sample.

2.4 Characterization of the implant surfaces

The chambers, including PLA, PLA + pDA, PLA + Tra, and PLA + pDA + Tra, were characterized in terms of surface roughness and wettability. The microscopic morphology of the surfaces was imaged using an S-3000N scanning electron microscope (SEM) (Hitachi, Tokyo, Japan). The average roughness (Ra) was determined with a confocal laser scanning microscope (Olympus, OLS4100, Japan), and the wettability of each implant was determined by the water contact angle (CA) on the surface with an optical contact angle meter (Dataphysics, OCA20, Germany).

2.5 Tranilast-release behavior in a rough PLA + pDA + Tra chamber

To evaluate the *in vitro* tranilast-release behavior, the PLA + pDA + Tra and PLA + Tra chambers were each immersed in PBS with a pH of 7.5, incubated at 37 °C with moderate agitation for 30 days, 20 ml of medium was withdrawn every three days and the same volume of fresh buffer was poured back to maintain the same sink condition. The absorbance of the harvested medium was measured using a spectrophotometer at a wavelength of 335 nm. Each experiment was repeated three times and the data were plotted as a percentage of cumulative drug release using the following eqn (1):

$$Y_n = \frac{Y_{n-1} + (C_n \times 100\ (\mathrm{ml}) - C_{n-1} \times 80\ (\mathrm{ml}))}{\text{Initial tranilast loading mess(ug)}} \times 100\% \quad (1)$$

where Y_n and C_n denote the cumulative tranilast release proportion and tranilast concentration in the medium at the nth sampling time (%, μg ml^{-1}), respectively; $Y_0 = 0$.

2.6 The effect of varied treatments on fibroblast morphology and proliferation

Rabbit skin fibroblast cells were purchased from ScienCell Research Laboratories (Rab2300, USA) and cultured in high-glucose Dulbecco's modified Eagle's medium (DMEM) containing 10% fetal bovine serum (FBS). Fibroblasts were infected with GFP, divided into four groups, and plated in 6-well plates. Group 1 was the control group with PLA, group 2 was PLA + pDA, group 3 was PLA + Tra, and group 4 was PLA + pDA + Tra treatment. Fibroblasts were planted on the surface of each material at a density of 2×10^5. After 48 h of incubation in the medium, the fibroblasts were examined and photographed under a fluorescence microscope (Olympus, Germany) to detect the adhesion morphology.

The proliferation of fibroblasts was determined by the standard MTT assay. Briefly, fibroblasts were seeded in 96-microwell plates (3000 cells/well). After 24 h of culture, PLA, PLA + pDA, PLA + Tra, and PLA + pDA + Tra, were added to each well and normal saline (0.9%) as a negative control. After incubating for another 24 h, the treated cells were washed with PBS (pH 7.4, 0.01 M), and then 200 μL of MTT solution (500 μg ml^{-1}, Beijing Soleibao Technology Co., Ltd.) was added and incubated for 4 h in the dark. After the medium was removed, 150 μL of DMSO was added to each well and incubated for another 10 min. The absorbance of the solutions was measured at 490 nm using a microplate spectrophotometer (Tecan Spark).

2.7 Animals and surgery

All animal experiments were approved by the Animal Protection Committee of Nanfang Hospital and performed following the guidelines of the National Health and Medical Research Committee. Adult female New Zealand rabbits ($n = 96$, weighing 2.5–3.0 kg) were selected for this study. Prior to surgery, the animals were raised in a dedicated pathogen-free room with a 12 h day–night cycle and fed a routine diet.

The animals were randomly divided into four groups: Group 1 was set as the control group with PLA chamber, group 2 was PLA + pDA chamber, group 3 was PLA + Tra chamber, and group 4 was rough PLA + pDA + Tra chamber ($n = 24$ in each group). Animals were anesthetized by intramuscular injection of sodium pentobarbital (2 mg kg^{-1}), then the upper back skin was shaved and sterilized with 75% ethanol. From the suprascapular region, a longitudinal incision (length = 10 cm) was made in the suprascapular region. Then, the subcutaneous fascia layer was then ruptured by blunt and sharp dissection to reveal the inferior fat flaps, which were nourished by pairs of independent blood vessels from the deeper muscle tissues. The distal fat flap (approximately 1 ml was dissected carefully with a pedicled vessel connected to the original branch and unbounded by removing the external fascia. To prevent inadvertent retraction, the harvested flap was inserted into the chamber and pulled to the opposite side with the suture, and the chamber and flap tail were anchored to the nearby myofascial membrane. After the surgical area was washed with sterile saline solution, the wound was closed and the animals were returned to the cage.

2.8 Magnetic resonance imaging to detect the neo-formed tissue

After anesthesia, to ensure analgesia throughout the procedure, the rabbits were imaged with magnetic resonance imaging (MRI) using a 0.2T (Hitachi, Airis Mate) or 7T (Bruker, Biospec, Ettlingen, Germany) imaging system to determine the volume of the fat flap. The layer thickness of the 3D sequence was set to 5 or 2 mm, and T1, T2, T13D, and T1WI images were collected. Post-processing of the MRI images, including three-dimensional reconstruction and volume measurement, was performed by three independent operators using ITK-SNAP 3.2 software.

2.9 Tissue harvest and histological analyses

Animals were randomly selected and anesthetized after 0, 4, 8, and 16 weeks (6 at each time point). The fat flaps, including the chamber, were harvested from the chamber. Fat tissue was fixed in neutral-buffered formalin and embedded in paraffin. Four micrometer-thick sections were stained with hematoxylin and

eosin and Masson's trichrome stain. Fibrosis-positive areas were measured using ImageJ (National Institutes of Health, Bethesda, MD, United States).

For immunofluorescence analyses, fat tissue sections were incubated with the following primary antibody: mouse anti-rabbit α-SMA (1 : 100, Abcam). The number of α-SMA-positive cells per field was then counted.

2.10 Real-time quantitative polymerase chain reaction

RNA isolated and quantified from the fat flaps in the four groups was used to synthesize cDNA using PrimeScript™ RT Master Mix (TaKaRa, Kyoto, Japan). PCR was performed using a LightCycler 480 Real-time PCR System (Roche, Indianapolis, IN, USA) and SYBR Premix Ex Taq (TaKaRa). Expression levels were calculated using the $2^{-\Delta\Delta CT}$ method. The following primers were used.

	F	R
SDF-1	CCCACCATCTACTCCATCA	GAAATCGGGAATAGTCAGC
TGF-β	AGCTGTACATTGACTTCCGCA	CAGGCAGAAGTTGGCGTGGT
C/EBPα	GATCCTGATCTGCGCAATAG	AATTCAGCCTTTGAGCTCATT
PPARγ	GGCTTCCACTATGGAGGTCAT	GAGGACCCCGTCTTTATTCAT
β-actin	TCCTGCGTCTGGACCTGG	GCCCGACTCGTCATACTCC

2.11 Statistical analysis

All data are expressed as mean ± SD. According to the experimental grouping design, a one-way analysis of variance was used for the statistical analysis of data between groups at a specific time, and a two-way analysis of variance was used for the statistical analysis of data between groups at different times. A value of $p < 0.05$ was considered statistically significant.

3. Results

3.1 Mechanical characterization of the 3D printed PLA chamber

First, a three-point bending test was performed to evaluate the mechanical properties of the 3D printed chamber (Fig. 2a and b). The curves in Fig. 2c show the load–displacement profile of the 3D-printed PLA chamber.

3.2 Surface characterization of the 3D printed PLA chambers

The surface topographies of PLA, PLA + pDA, PLA + Tra, and PLA + pDA + Tra were analyzed using SEM (Fig. 3). After coating with pDA, the PLA + pDA sample was covered with small spherical particles. The surface topography of the substrates was also affected by the tranilast coating, and a large amount of tranilast envelope was found on the PLA + Tra and PLA + pDA + Tra samples.

3.3 Surface roughness (Ra) of the samples in the different groups

A confocal laser scanning microscope (Fig. 4a) was used to measure the average roughness (Ra). As shown in Fig. 4c the lowest Ra was obtained for the PLA surface and the highest for the PLA + pDA + Tra surface.

3.4 Water contact angle (CA) of the samples from the different groups

Fig. 4b and d clearly show the hydrophilic performance of the samples. As expected, the hydrophilicity of the membranes improved with the adhesion of the different proteins. The PLA + pDA, the PLA + Tra, and the PLA + pDA + Tra surfaces were found to be highly hydrophilic materials, indicating

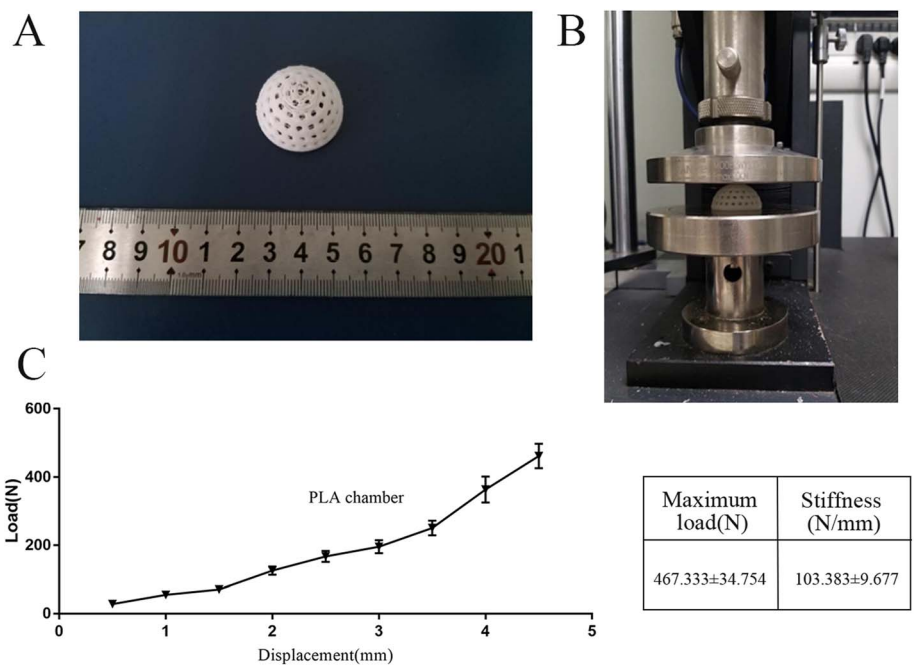

Maximum load(N)	Stiffness (N/mm)
467.333±34.754	103.383±9.677

Fig. 2 Mechanical characterization of the 3D printed PLA chamber (A and B) the load–displacement curves of smooth silicone and PLA chamber; (C) representation of the maximum load and stiffness of the different chambers ($n = 5$).

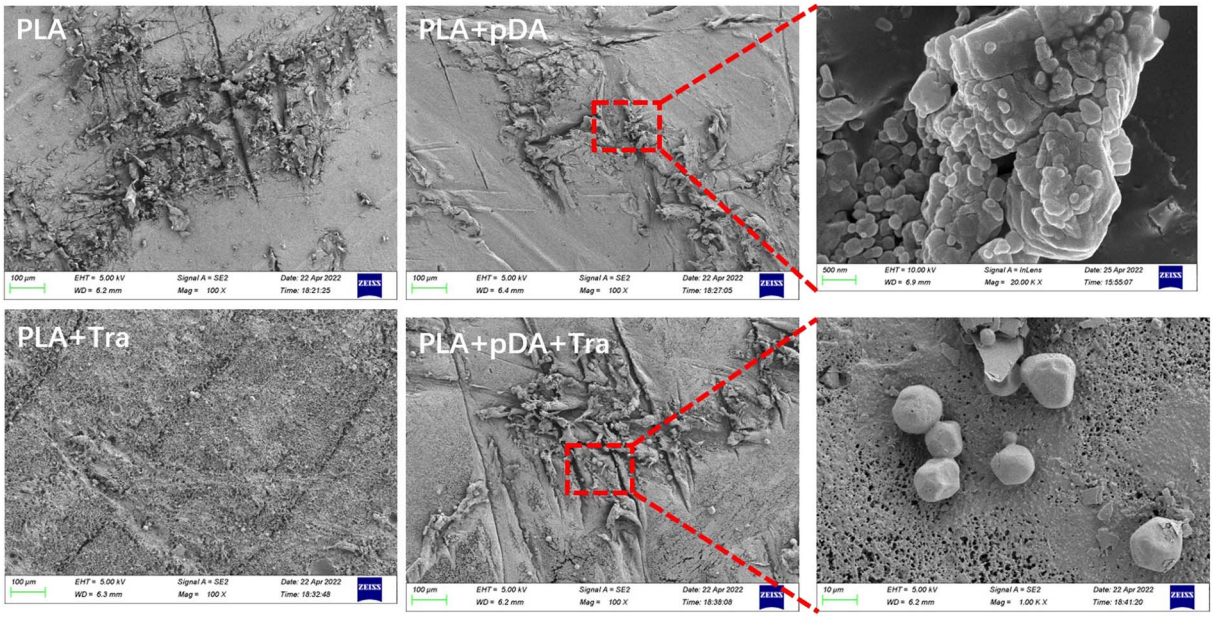

Fig. 3 Scanning electron microscopy (SEM) of pDA or Tra on the surface of PLA of the four samples.

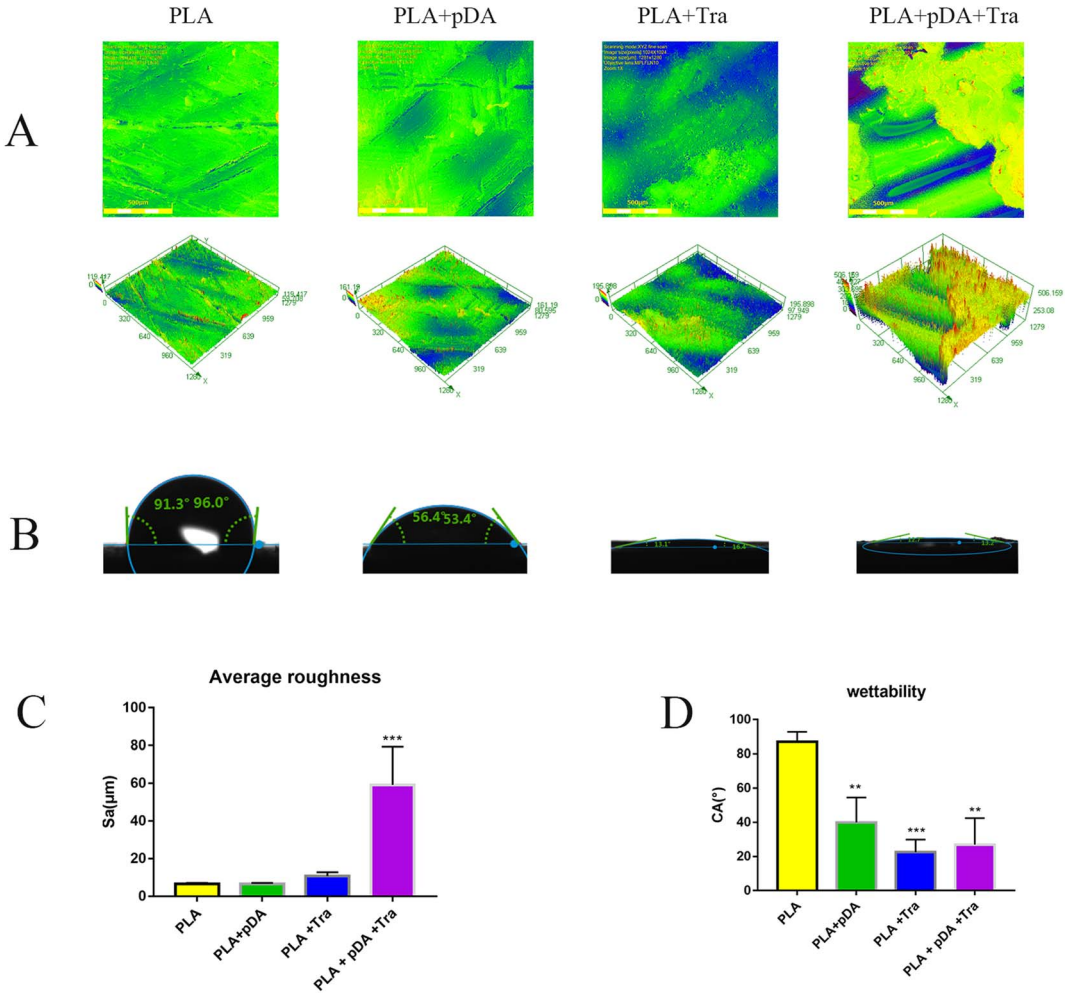

Fig. 4 Characterization of four samples with distinct surface roughness and contact angle. (A) Two-dimensional graphics and three-dimensional graphics of the sample surfaces using the confocal laser scanning microscopy Image, scale bars = 500 μm; (B) contact angle of the four surfaces; (C) the quantified values of average roughness (Ra) and (D) the quantified values of contact angle (CA). $^{**}p < 0.01$, $^{***}p < 0.001$ *versus* PLA group.

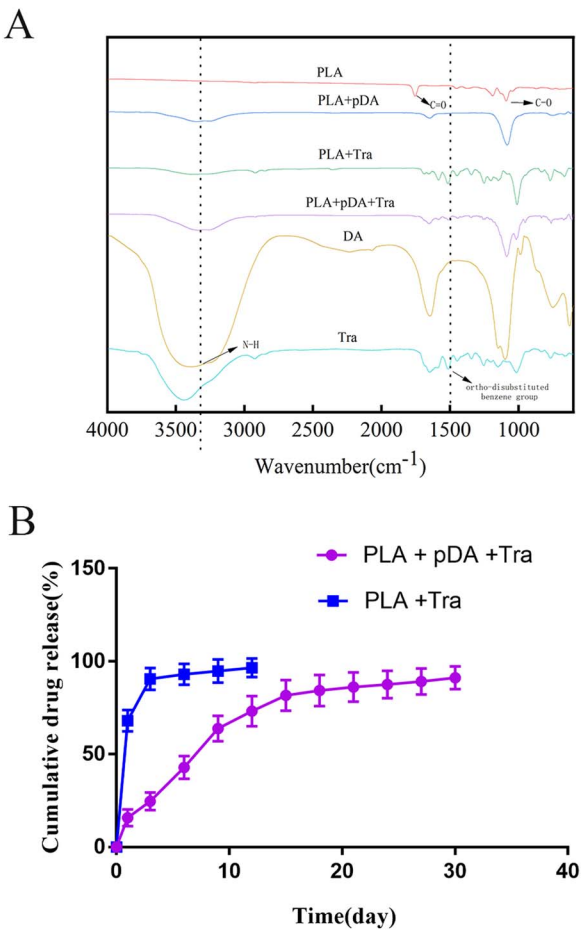

Fig. 5 FI-TR spectrum and Tra release of samples. (A) FI-TR spectrum of PLA, PLA + pDA, PLA + Tra, PLA + pDA + Tra, DA and Tra; (B) the release profile of tranilast on PLA + Tra and PLA + pDA + Tra samples (n = 5).

a significant increase in wettability due to the pDA or tranilast coating of the substrates.

3.5 FTIR spectrum of the samples in different groups

The FTIR spectra of PLA, PLA + pDA, PLA + Tra, and PLA + pDA + Tra are shown in Fig. 5a. The dashed lines show the characteristic peaks of interest. For the intact tranilast, there was a characteristic peak near the wavelength of 1500 cm^{-1}, attributed to an ortho-disubstituted benzene group.[27] The characteristic peak of dopamine at 3340 cm^{-1} is attributed to the active N–H primary amine stretching present on the dopamine molecule.[28] PLA exhibits a carbonyl stretching band at 1740 cm^{-1}.[29] In the FTIR spectra of the coated samples, the characteristic peaks of each constituent overlap, indicating that the coated samples contain their own constituents. In other words, there are characteristic peaks of PLA and dopamine in the PLA + pDA spectra. Characteristic peaks originating from PLA and tranilast were also observed in the PLA + Tra spectra. In addition, the PLA + pDA + Tra spectra showed characteristic peaks for all three components.

3.6 *In vitro* profile of sustained release of PLA + pDA + Tra samples

The sustained release of tranilast on PLA + pDA and PLA was followed for 30 days. As shown in Fig. 5b, tranilast was rapidly released from PLA during the first 3 days (90.5 ± 5.95%). Thereafter, tranilast continued to be released slowly from PLA. In contrast, it was rapidly released from PLA + pDA within 15 days, and the sustained release rate of the drug was relatively stable from day 12 to day 30 so that by the end of day 30, almost 91.17% of the tranilast had been released. The above results suggest that with dopamine's assistance, the whole platform has long-lasting drug release characteristics, close to the first-

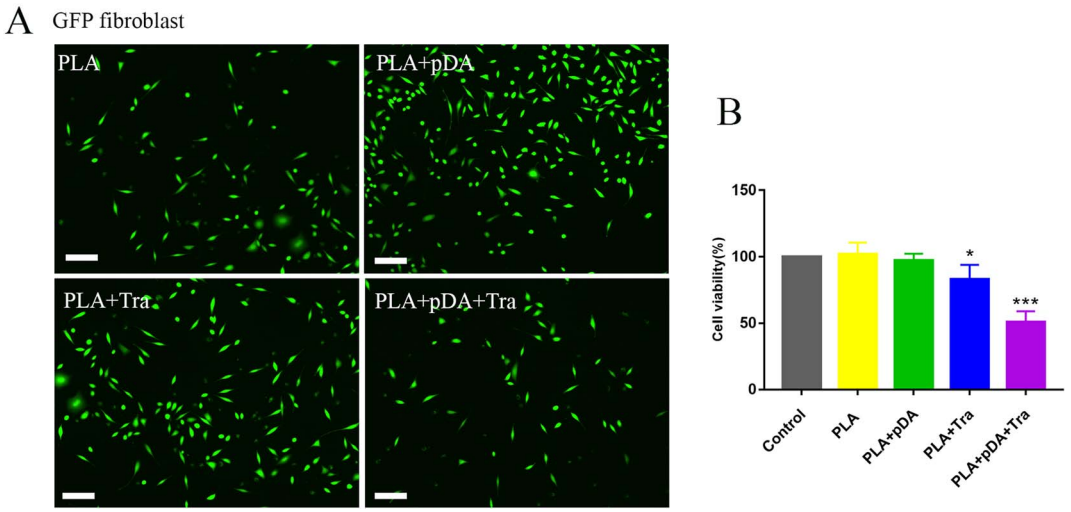

Fig. 6 PLA + pDA + Tra sample attenuated the fibroblast adhesion and the proliferation of fibroblasts. (A) The adhesion behavior of the cells and morphological response to the different treatments; (B) the quantitative analysis of the proliferation of fibroblasts. *p < 0.05, ***p < 0.001; scale bars = 50 μm (n = 6).

order release mode, resulting in a sustained anti-fibrosis effect *in vivo*.

3.7 The effect of PLA + pDA + pTra on the adhesive function of fibroblasts

Cell adhesion was imaged using a fluorescence microscope, as shown in Fig. 6a. Quantification showed that PLA + pDA attracted the highest density of fibroblasts. PLA + pDA + Tra could significantly affect the adhesion behavior as the cell numbers decreased dramatically, which could be due to the rough surface (Fig. 6b), suggesting that tranilast loading could further decrease the adhesion of fibroblasts.

3.8 Volume and morphological evaluation of artificial adipose tissue

The chambers of the four groups, PLA, PLA + pDA, PLA + Tra, and PLA + pDA + Tra, were implanted into the animals with pedicled fat flap transplantation as in the previous TEC protocols (Fig. 7a), The newly formed artificial adipose tissues were imaged by MRI and the volume rendering is shown in Fig. 7b and c. The tissue gradually expanded over time starting from a baseline value of 1 ml, with a dramatic increase in the increasing trend, reaching a plateau at 8 weeks in the PLA chamber. At this time, the fat flap volumes of PLA, PLA + pDA, PLA + Tra, and PLA + pDA + Tra were 3.283 ± 0.286, 3.4 ± 0.316, 3.433 ± 0.294, and 3.417 ± 0.286 ml, respectively, and no

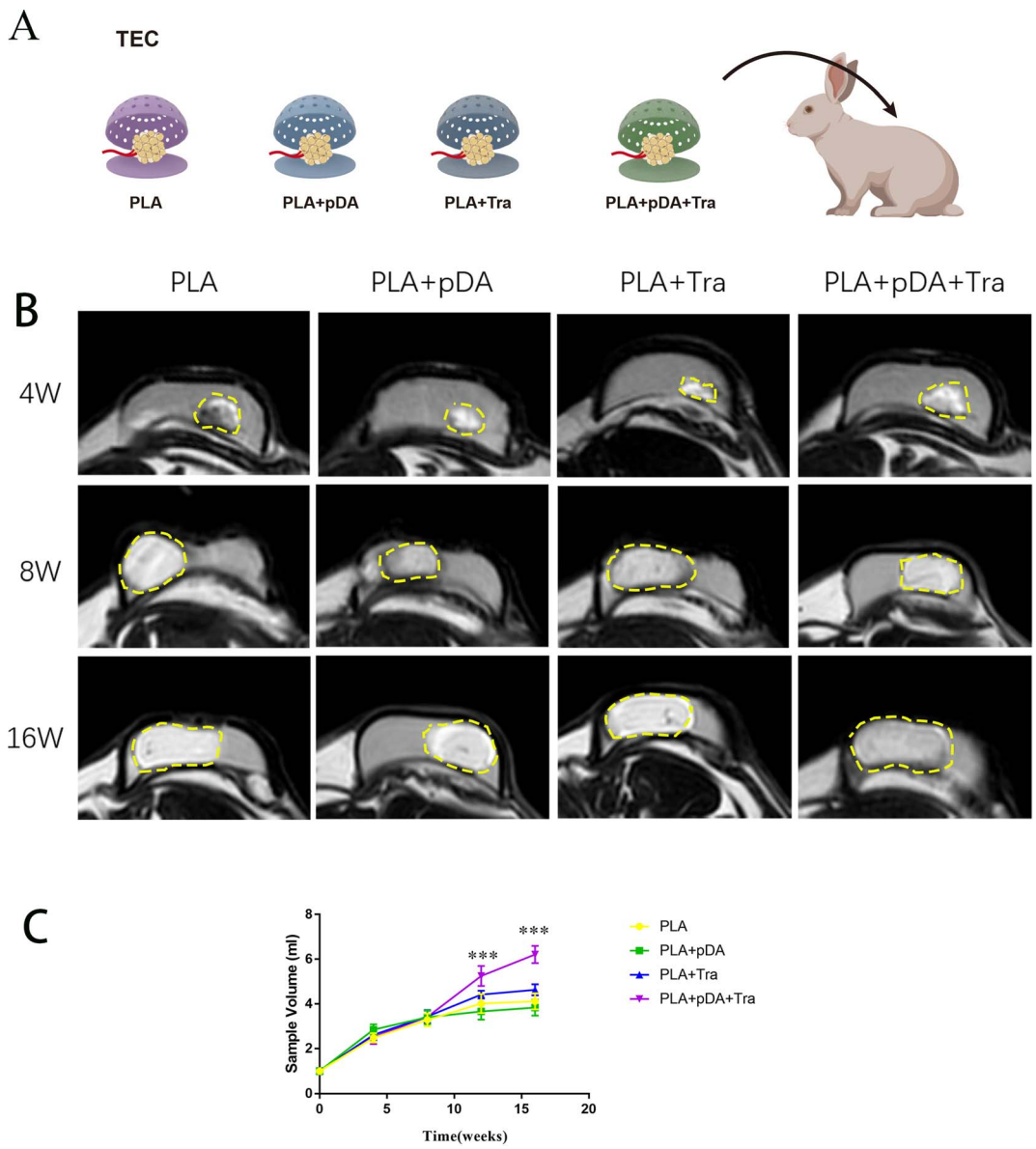

Fig. 7 PLA + pDA + Tra chamber generated large volume tissue. (A) Schematic of TEC experiments with different chambers: PLA, PLA + pDA, PLA + Tra, and PLA + pDA + Tra, the pedunculated fat flaps were dissected and implanted into the chambers to serve as primary seeds for adipose tissue regeneration ($n = 24$); (B) MRI and three-dimensional reconstruction techniques were used to evaluate the volume of newly formed tissues (yellow dotted line); and (C) the quantitative volume of neo-formed tissue in the different groups. ***$p < 0.001$ *versus* PLA group.

statistically significant difference between the groups was found. After 8 weeks, the fat flap volume of the PLA slightly increased; however, the newly formed tissue in the rough PLA + pDA + Tra chamber increased continuously with time, reaching 6.208 ± 0.388 ml after 16 weeks.

3.9 Histological analysis of the artificial adipose tissue

Histological staining was performed to show the process of artificial adipose tissue and the efficiency of physical-chemical modification in each group (Fig. 8a). The results showed that abundant connective tissue was found in the fat flaps of the four groups after 4 weeks. After 16 weeks, vascularized and well-organized adipose tissue was developed in the PLA + pDA + Tra chamber, which was mature adipose tissue with supporting blood vessels, and connective tissue decreased. However, neo-forming connective tissue was still present in the other groups, especially in the PLA chamber group (Fig. 8b).

The major transcription factors for adipogenic differentiation, C/EBPα and PPAR-γ (Fig. 8c and d), were further tested using Q-PCR. The results showed that adipogenesis was still strong in the PLA + pDA + Tra chamber even at the later stage of the construction (8 to 16 weeks). This was significantly higher than that in the PLA group, indicating that the PLA group loaded with pDA + Tra could continue to promote adipogenic differentiation.

3.10 Assessment of capsule formation and fibrosis in the engineered adipose tissue

The degree of fibrogenesis, the capsule thickness, and the function of the myofibroblast in the engineered fat flap were assessed. The results in Fig. 9a show that the collagen fibers dominated the capsular component and were aligned in parallel in each group after 16 weeks. Quantitative analysis showed that the fibrous capsule in the PLA + pDA + Tra chamber was the thinnest (74.83 ± 6.91 μm), which was less than that of the PLA (203.2 ± 21.32 μm) (Fig. 9c). Moreover, there were plenty of α-SMA-positive myofibroblasts in the PLA capsule, which were uniformly arranged in parallel in the thick capsule (Fig. 9b). Nevertheless, the distribution of positive cells on the PLA surface was random and disordered, and the number of luminescent cells in the PLA + pDA + Tra group was significantly lower than that in the PLA, PLA + pDA, and rough PLA + Tra groups (Fig. 9d). The mRNA levels of SDF-1 (Fig. 9e) were not significantly different between the groups, but TGFβ (Fig. 9f)

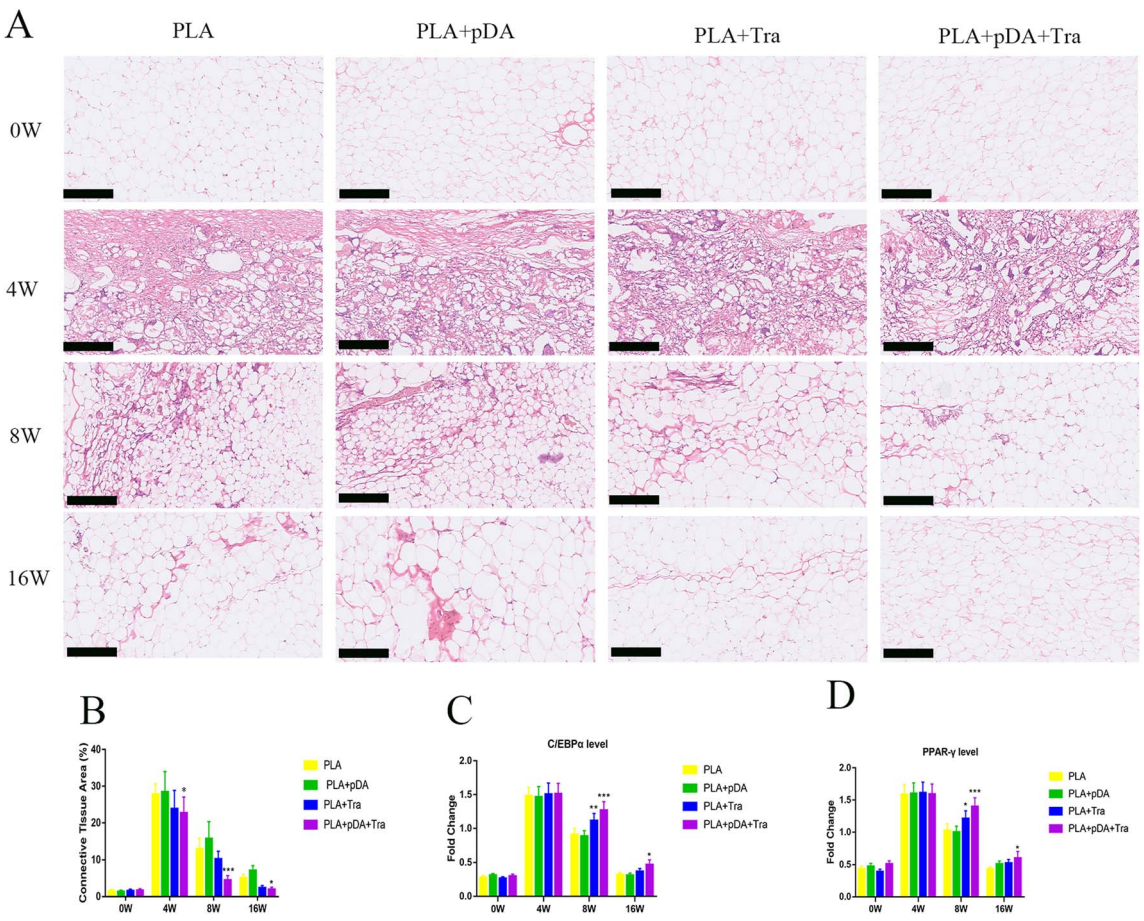

Fig. 8 The decreased fibrosis and continuous adipogenesis in PLA + pDA + Tra chamber. (A) The HE staining of and (B) the amount of connective tissue areas in adipose tissue in different chambers; the adipogenic gene expression of (C) C/EBPα and (d) PPARγ in the different groups at the designated time point by Q-PCR. *$p < 0.05$,**$p < 0.01$, ***$p < 0.001$ *versus* PLA group at the same time; scale bars = 250 μm.

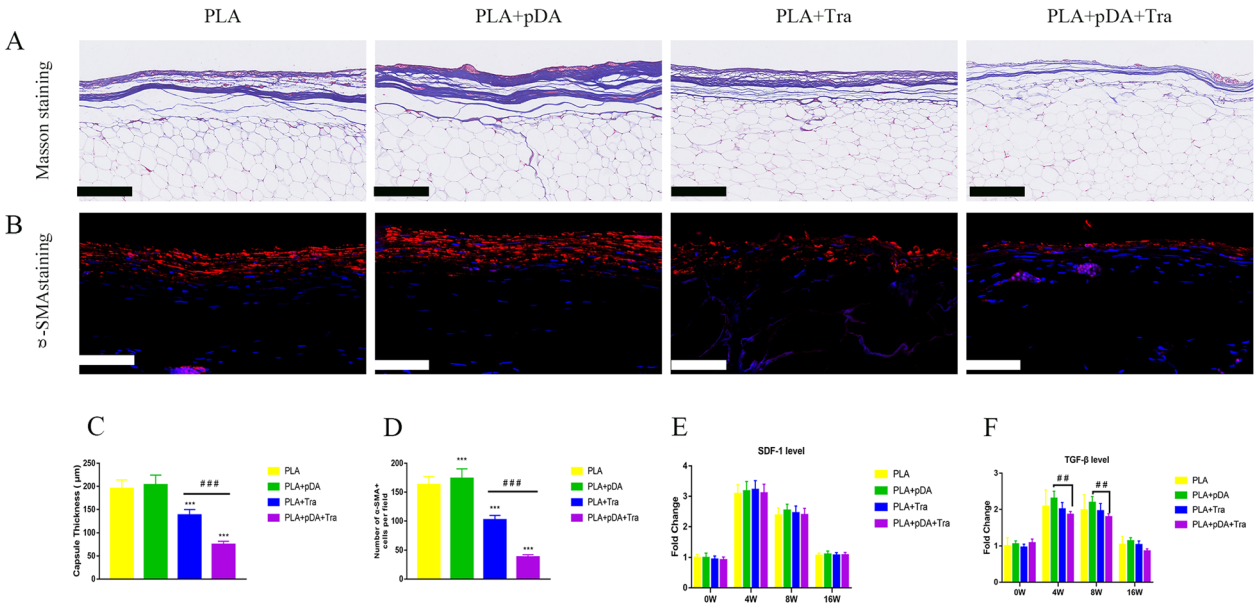

Fig. 9 PLA + pDA + Tra chamber attenuated the capsule formation *in vivo*. (A) the Masson staining and (B) the microscopic images of α-SMA staining; (C) capsule thickness in the different groups at 16 weeks and (D) the number of positive cells in newly formed tissues; (E) the SDF-1 and (F) TGF-β expression in different groups at the designated time point by Q-PCR. $^{**}p < 0.01$, $^{***}p < 0.001$ *versus* PLA group at the same time; Scale bar = 250 μm.

showed a significantly attenuated expression in the rough PLA + pDA + Tra chamber than in the other three groups.

4. Discussion

In this study, we used PLA as a substrate and fabricated the desired shapes by 3D printing. We then rubbed the chamber to obtain a rough surface, and the final anti-fibrosis layer was achieved by coating tranilast with the assistance of pDA. *In vitro* and *in vivo* tests were performed to demonstrate the anti-fibrosis efficacy. Chamber implantation and histological assessment confirmed the large-volume regeneration of the mature fat flap attributed to the PLA + pDA + Tra chamber (Fig. 10). The results can be summarized as follows: (1) compared with the PLA chamber, the PLA + pDA + Tra chamber was able to induce the continuous expansion of the fat flap and significantly increase the final volume; (2) the release of tranilast showed long-lasting kinetics benefiting from the support of the pDA adhesive layer to ensure its efficacy until the later period of remodeling with an inhibitory effect on fibrosis or capsule formation accompanied by myofibroblast polarization.

The physiological process of adipose tissue regeneration induced by the TEC technique includes three independent but overlapping phases:[9,10,30] aseptic inflammation, adipocyte hyperplasia and hypertrophy, and the final period of adipose tissue remodeling. Aseptic inflammation persists mainly until 4 weeks after the chamber implantation and fat flap dissection, activating nonspecific inflammation, and seed cell reservoir for the subsequent adipocyte hyperplasia. Thereafter, the adipose precursor cells continuously differentiated into adipocytes due to the adipogenic environment created by the implanted fat flap, after which the extracellular matrix was remodeled under the conditions of inner adipose expansion and fibrosis. During these later phases, the outer capsule forms rearrange, and contracts centripetally, thereby, impeding the thriving of the engineered fat flap. The final thickness and strength of the capsule were closely related to the overall regenerative environment and corresponded to the final volume. Therefore, we focused on manipulating fibrosis formation to achieve a larger volume of engineered adipose tissue.

It is worth noting that PLA was selected as the chamber material in this study. Currently, most existing TECs are permanent and have the inherent limitation of leaving a foreign material within the body. Permanent TECs could lead to the development of chronic adverse host responses, such as chronic inflammation with prominent alteration of surrounding tissues leading to an abundant fibrotic capsule. The permanent silicone was used for TEC applications in our previous studies, but it induced major foreign body reactions,[31] due to the overexpression of TGF-β during persistent chronic inflammation. PLA is the most widely studied and practical biodegradable aliphatic polyester.[32,33] In this study, tissue engineering chambers with a delicate design were prepared using a 3D printer based on a fused deposition modeling technique, which can withstand skin tension better than conventional silicone. We also found that the PLA chambers were already partially degraded after the removal from the animals (data not shown). Most studies have confirmed the complete degradation of PLA. Regarding a suitable degradation time in the chamber model, further research is needed to prepare a synthetic PLA chamber by the copolymer method or other solutions that correspond to our clinical schedule in which the chamber is preferably degraded after the proliferation time. In this way, the mature

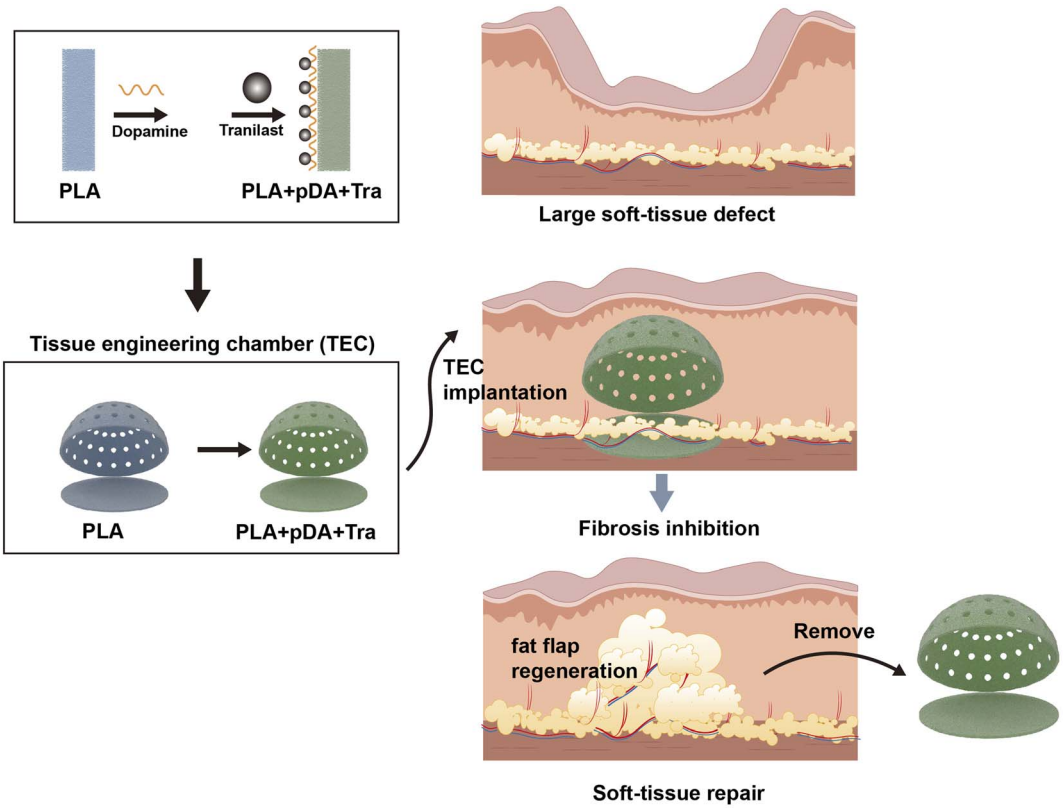

Fig. 10 The schematic representation of large adipose tissue regeneration by PLA + pDA + Tra chamber.

adipose tissue could be produced in one step with gradual degradation of the chamber.

The surface properties of biological materials such as roughness, texture, surface free energy, surface charge, and chemical composition affect the migration and adhesion of inflammatory cells. For example, a rough interface can significantly reduce the adhesion and proliferation of fibroblasts; in contrast, these cells tend to migrate on a smooth surface.[21,34] The surface topography of the substrates was affected by the pDA or Tra coating, as reported by Wang,[26] and pDA coating significantly changed the microtopography of the substrate. We also demonstrated in the current report that, pDA + Tra coating can further increase the roughness of the substrate and inhibit the adhesion of fibroblasts to a greater extent, compared with PLA.

The efficacy of TECs in the generation of large-volume adipose tissue has been reported. To provide sufficient tissue volumes, TEC was utilized either alone or in combination with flaps. However, this technique may occasionally result in capsular contracture. To avoid fibrous capsules, antifibrotic drug strategies were used in conjunction with TEC. For example, a sustained basic fibroblast growth factor (bFGF) drug delivery system facilitated large volume soft fat tissue regeneration and reduced fibrous capsule formation.[35] Among the strategies for various tissue and organ regeneration, Tra for inhibiting fibrosis formation has been extensively investigated.[36] For example, a sustained Tra delivery system that is based on poly(lactic-*co*-glycolic acid) (PLGA) is capable of effectively preventing fibrosis.[37] Chien *et al.* revealed that Tra-loaded microneedle (TMN) was effectively applied in a rabbit ear model to treat induced hypertrophic scars, and the expression of transforming growth factor-β, collagen-1, and α-smooth muscle actin proteins was reduced in TMN-treated HSs compared to the control.[38]

Moreover, during the gradual formation and densification of the capsule, not only the migration and enrichment of fibroblasts are involved, but also the activation of fibroblasts and their polarization into myofibroblasts are also crucial for capsular densification.[19] The violent collagen synthesis period in these cells is a key feature of cellular type transformation and is also characterized by a high level of extracellular vesicles together with stress fibers. Regarding the protein profile, adhesive protein is synthesized in the early stage of the transformation, and smooth muscle actin appears in the later stage.[20] Macrophages are mainly involved in the synthesis of TGF-β during chronic inflammation. This late production of TGF-β promotes the recruitment and proliferation of fibroblasts and collagen synthesis, these phenomena are associated with the formation of a thick fibrous capsule around the implant. tranilast, as an effective drug for inhibiting scar hyperplasia, has been shown to bind specifically to TGF-β1 receptors and inhibit the activation of pro-fibrotic signals, such as TGF-β-mediated Smad, Wnt/β, and Hippo YAP/TAZ.[39] However, tranilast is difficult to adhere to the surface of the hydrophobic structure, thus affecting subsequent drug release and effect.

Dopamine contains abundant catechol and amine functional groups and its self-polymerization process involves the oxidative conversion of catechol to quinone, which further conjugates with amines, imidazole, or thiol groups to form ultra-thin adhesive pDA films. In our previous research, it was successfully proved that the pDA coating has good adhesion properties as such pDA can form good adhesion and increase drug loading. We observed that the PLA + pDA + Tra group had good Tra release characteristics *in vitro*, and the release process could last for nearly one month.

Therefore, we attempted to build a tranilast layer on the rough PLA surface to further enhance the anti-fibrotic effect. In general, the drug cannot directly adhere to the surface of the PLA substrate due to partial hydrophobicity. We had previously enriched platelets on the biomaterial surface with a polydopamine coating to achieve a growth factor sustain-release system.[40] Therefore in the present study, a polydopamine coating with strong and universal adhesion to the PLA surface was used, and its drug release kinetics *in vitro* and the inhibitory effect on the transformation of fibroblasts to myofibroblasts *in vivo* were investigated.

In summary, surface modification and tranilast loading into the PLA chamber can effectively inhibit fibrosis formation, which is crucial for achieving large-scale adipose tissue regeneration. Despite the encouraging results of our study, there is still a gap between laboratory results and clinical practice. Further work is needed to develop more suitable chamber materials, such as modification of degradable materials, better drug embedding and release, and controlled and complete degradation at the desired time.

5. Conclusions

We reported a dopamine-based tissue engineering system that used a tranilast-loaded PLA chamber for adipogenesis through reducing the formation of tissue fibrosis. The PLA + pDA + Tra showed good drug loading and release characteristics. As compared to the PLA alone, the PLA + pDA + Tra chamber can significantly inhibit fibrosis in the newborn tissue and increase the volume of mature fat. These findings highlight the advantages of combining polydopamine-assisted tranilast release therapy and a biodegradable PLA chamber to achieve more effective fat regeneration results and provide a new idea for the clinical practice of breast reconstruction after tumor surgery.

Ethics statement

The animal study was reviewed and approved by the Animal Protection Committee of Nanfang Hospital.

Data availability statement

The raw data supporting the conclusions of this article will be made available by the authors, without undue reservation.

Author contributions

All authors listed have made a substantial, direct, and intellectual contribution to the work, and approved it for publication.

Conflicts of interest

The authors declare that they have no known competing financial interests or personal relationships that could have appeared to influence the work reported in this paper.

Acknowledgements

This work was financially supported by the following foundation: National Natural Science Foundation of China (Grant number: 81772101, 82072196, 82002066). We also thank the support from the Science Fund for Distinguished Young Scholars of Southern Medical University (Grant number: 2020J009).

References

1 C. Y. Lumpkins, A. Philp, K. L. Nelson, L. M. Miller and K. A. Greiner, A road map for the future: An exploration of attitudes, perceptions, and beliefs among African Americans to tailor health promotion of cancer-related genetic counseling and testing, *J. Genet. Couns.*, 2020, **29**(4), 518–529.

2 P. M. A. Breast, reconstruction, *Obstet. Gynecol. Clin. North Am.*, 2002, **1**(29), 209–223.

3 A. S. Colwell and E. M. Taylor, Recent Advances in Implant-Based Breast Reconstruction, *Plast. Reconstr. Surg.*, 2020, **145**(2), 421e–432e.

4 X. Zhang, L. Cai, B. Yin, X. Han and F. Li, Total breast reconstruction using large-volume condensed and viable fat grafting after mastectomy, *J. Plast., Reconstr. Aesthetic Surg.*, 2021, **74**(5), 966–973.

5 D. Ajdic, Y. Zoghbi, D. Gerth, Z. J. Panthaki and S. Thaller, The Relationship of Bacterial Biofilms and Capsular Contracture in Breast Implants, *Aesthetic Surg. J.*, 2016, **36**(3), 297–309.

6 Q. Z. Ruan, J. R. Rinkinen, A. F. Doval, B. B. Scott, A. M. Tobias, S. J. Lin, *et al.*, Safety Profiles of Fat Processing Techniques in Autologous Fat Transfer for Breast Reconstruction, *Plast. Reconstr. Surg.*, 2019, **143**(4), 985–991.

7 A. Messina, S. K. Bortolotto, O. C. S. Cassell, J. Kelly, K. M. Abberton and W. A. Morrison, Generation of a vascularized organoid using skeletal muscle as the inductive source, *FASEB J.*, 2005, **19**(11), 1570–1572.

8 J. H. Dolderer, K. M. Abberton, E. W. Thompson, J. L. Slavin, G. W. Stevens, A. J. Penington, *et al.*, Spontaneous Large Volume Adipose Tissue Generation from a Vascularized Pedicled Fat Flap Inside a Chamber Space, *Tissue Eng.*, 2007, **13**(4), 673–681.

9 M. W. Findlay, J. H. Dolderer, N. Trost, R. O. Craft, Y. Cao, J. Cooper-White, *et al.*, Tissue-engineered breast reconstruction: bridging the gap toward large-volume tissue engineering in humans, *Plast. Reconstr. Surg.*, 2011, **128**(6), 1206–1215.

10 Z. Peng, Z. Dong, Q. Chang, W. Zhan, Z. Zeng, S. Zhang, *et al.*, Tissue engineering chamber promotes adipose tissue regeneration in adipose tissue engineering models through induced aseptic inflammation, *Tissue Eng., Part C*, 2014, **20**(11), 875–885.

11 H. Debels, J. Palmer, X. L. Han, C. Poon, K. Abberton and W. Morrison, In vivo tissue engineering of an adipose tissue flap using fat grafts and Adipogel, *J. Tissue Eng. Regener. Med.*, 2020, **14**(4), 633–644.

12 R. Song, M. Murphy, C. Li, K. Ting and C. Soo, Current development of biodegradable polymeric materials for biomedical applications, *Drug Des., Dev. Ther.*, 2018, **12**, 3117–3145.

13 B. Tyler, D. Gullotti, A. Mangraviti, T. Utsuki and H. Brem, Polylactic acid (PLA) controlled delivery carriers for biomedical applications, *Adv. Drug Delivery Rev.*, 2016, **107**, 163–175.

14 M. S. Singhvi, S. S. Zinjarde and D. V. Gokhale, Polylactic acid: synthesis and biomedical applications, *J. Appl. Microbiol.*, 2019, **127**(6), 1612–1626.

15 G. Li, M. Zhao, F. Xu, B. Yang, X. Li, X. Meng, *et al.*, Synthesis and Biological Application of Polylactic Acid, *Molecules*, 2020, **25**(21), 5023.

16 S. W. Jordan, J. E. Fligor, L. E. Janes and G. A. Dumanian, Implant Porosity and the Foreign Body Response, *Plast. Reconstr. Surg.*, 2018, **141**(1), 103e–112e.

17 M. R. Major, V. W. Wong, E. R. Nelson, M. T. Longaker and G. C. Gurtner, The foreign body response: at the interface of surgery and bioengineering, *Plast. Reconstr. Surg.*, 2015, **135**(5), 1489–1498.

18 F. Taraballi, M. Sushnitha, C. Tsao, G. Bauza, C. Liverani, A. Shi, *et al.*, Biomimetic Tissue Engineering: Tuning the Immune and Inflammatory Response to Implantable Biomaterials, *Adv. Healthcare Mater.*, 2018, **7**(17), 1800490.

19 R. T. Hannan, S. M. Peirce and T. H. Barker, Fibroblasts: Diverse Cells Critical to Biomaterials Integration, *ACS Biomater. Sci. Eng.*, 2018, **4**(4), 1223–1232.

20 J. Baum and H. S. Duffy, Fibroblasts and myofibroblasts: what are we talking about?, *J. Cardiovasc. Pharmacol.*, 2011, **57**(4), 376–379.

21 B. R. Prasad, M. A. Brook, T. Smith, S. Zhao, Y. Chen, H. Sheardown, *et al.*, Controlling cellular activity by manipulating silicone surface roughness, *Colloids Surf., B*, 2010, **78**(2), 237–242.

22 F. See, M. Watanabe, A. R. Kompa, B. H. Wang, A. J. Boyle, D. J. Kelly, *et al.*, Early and Delayed Tranilast Treatment Reduces Pathological Fibrosis Following Myocardial Infarction, *Heart, Lung Circ.*, 2013, **22**(2), 122–132.

23 X. Li, J. Liu and X. Shang, Effect of tranilast on myocardial fibrosis in diabetes rats through TGF-beta/Smad pathway, *Minerva Med.*, 2021, **112**(1), 153–154.

24 M. Gyöngyösi, J. Winkler, I. Ramos, Q. T. Do, H. Firat, K. McDonald, *et al.*, Myocardial fibrosis: biomedical research from bench to bedside, *Eur. J. Heart Failure*, 2017, **19**(2), 177–191.

25 M. ROGOSNITZKY, R. DANKS and E. KARDASH, Therapeutic Potential of Tranilast, an Anti-allergy Drug, in Proliferative Disorders, *Anticancer Res.*, 2012, **32**(7), 2471–2478.

26 Z. Wang, L. Chen, Y. Wang, X. Chen and P. Zhang, Improved Cell Adhesion and Osteogenesis of op-HA/PLGA Composite by Poly(dopamine)-Assisted Immobilization of Collagen Mimetic Peptide and Osteogenic Growth Peptide, *ACS Appl. Mater. Interfaces*, 2016, **8**(40), 26559–26569.

27 S. Park, M. Park, B. H. Kim, J. E. Lee, H. J. Park, S. H. Lee, *et al.*, Acute suppression of TGF-ß with local, sustained release of tranilast against the formation of fibrous capsules around silicone implants, *J. Controlled Release*, 2015, **200**, 125–137.

28 D. Rohilla, S. Chaudhary, N. Kaur and A. Shanavas, Dopamine functionalized CuO nanoparticles: A high valued "turn on" colorimetric biosensor for detecting cysteine in human serum and urine samples, *Mater. Sci. Eng. C*, 2020, **110**, 110724.

29 S. Hassanajili, A. Karami-Pour, A. Oryan and T. Talaei-Khozani, Preparation and characterization of PLA/PCL/HA composite scaffolds using indirect 3D printing for bone tissue engineering, *Mater. Sci. Eng. C*, 2019, **104**, 109960.

30 W. A. Morrison, D. Marre, D. Grinsell, A. Batty, N. Trost and A. J. O'Connor, Creation of a Large Adipose Tissue Construct in Humans Using a Tissue-engineering Chamber: A Step Forward in the Clinical Application of Soft Tissue Engineering, *EBioMedicine*, 2016, **6**, 238–245.

31 L. Luo, Y. He, Q. Chang, G. Xie, W. Zhan, X. Wang, *et al.*, Polycaprolactone nanofibrous mesh reduces foreign body reaction and induces adipose flap expansion in tissue engineering chamber, *Int. J. Nanomed.*, 2016, **11**, 6471–6483.

32 S. Farah, D. G. Anderson and R. Langer, Physical and mechanical properties of PLA, and their functions in widespread applications - A comprehensive review, *Adv. Drug Delivery Rev.*, 2016, **107**, 367–392.

33 S. Stratton, N. B. Shelke, K. Hoshino, S. Rudraiah and S. G. Kumbar, Bioactive polymeric scaffolds for tissue engineering, *Bioact. Mater.*, 2016, **1**(2), 93–108.

34 S. Huang, Y. Chen, Q. Zhu, Y. Zhang, Z. Lei, X. Zhou, *et al.*, *In Vivo* and *In Vitro* Fibroblasts' Behavior and Capsular Formation in Correlation with Smooth and Textured Silicone Surfaces, *Aesthetic Plast. Surg.*, 2022, **46**(3), 1164–1177.

35 G. Zhang, H. Ci, C. Ma, Z. Li, W. Jiang, L. Chen, *et al.*, Additively manufactured macroporous chambers facilitate large volume soft tissue regeneration from adipose-derived extracellular matrix, *Acta Biomater.*, 2022, **148**, 90–105.

36 M. Kato, F. Takahashi, T. Sato, Y. Mitsuishi, K. Tajima, H. Ihara, *et al.*, Tranilast Inhibits Pulmonary Fibrosis by Suppressing TGFbeta/SMAD2 Pathway, *Drug Des., Dev. Ther.*, 2020, **14**, 4593–4603.

37 B. Kim, B. Huh, W. Lee, C. Kim, K. Lee, S. Nam, *et al.*, Silicone Implant Coated with Tranilast-Loaded Polymer in

a Pattern for Fibrosis Suppression, *Polymers*, 2019, **11**(2), 223.

38 P. N. Chien, J. H. Jeong, S. Y. Nam, S. Y. Lim, N. V. Long, X. R. Zhang, *et al.*, Nanomicelle-generating Microneedles Loaded With Tranilast for Treatment of Hypertrophic Scars in a Rabbit Model, *In Vivo*, 2022, **36**(4), 1734–1744.

39 J. Y. Chung, M. K. Chan, J. S. Li, A. S. Chan, P. C. Tang, K. Leung, *et al.*, TGF-β Signaling: From Tissue Fibrosis to Tumor Microenvironment, *Int. J. Mol. Sci.*, 2021, **22**(14), 7575.

40 S. Zhou, Q. Chang, F. Lu and M. Xing, Injectable Mussel-Inspired Immobilization of Platelet-Rich Plasma on Microspheres Bridging Adipose Micro-Tissues to Improve Autologous Fat Transplantation by Controlling Release of PDGF and VEGF, Angiogenesis, Stem Cell Migration, *Adv. Healthcare Mater.*, 2017, **6**(22), 1700131.